Journal of Organometallic Chemistry 760 (2014) 212–223

Contents lists available at ScienceDirect

Journal of Organometallic Chemistry

journal homepage: www.elsevier.com/locate/jorganchem

# $Cu^{II}$–salan compounds: Synthesis, characterization and evaluation of their potential as oxidation catalysts

Pedro Adão [a,*], Sónia Barroso [a], Fernando Avecilla [b], M. Conceição Oliveira [a], João Costa Pessoa [a,*]

[a] Centro de Química Estrutural, Instituto Superior Técnico, Universidade de Lisboa, Av. Rovísco Pais, 1049-001 Lisboa, Portugal
[b] Departamento de Química Fundamental, Universidade da Coruña, Campus de A Zapateira, 15071 A Coruña, Spain

ARTICLE INFO

*Article history:*
Received 3 September 2013
Received in revised form
10 October 2013
Accepted 11 October 2013

*Keywords:*
Copper
Reduced Schiff base
Salan
Oxidation catalysts
Sulfoxidation
Asymmetric catalysis

ABSTRACT

We report the synthesis and characterization of several salan-type $Cu^{II}$ complexes. Suitable crystals suitable for X-ray diffraction were obtained for several of the $Cu^{II}$ complexes, including a "half-salen" compound, revealing square-planar coordination environments common to $d^9$ species. The $Cu^{II}$–salan complexes are tested as catalysts in sulfoxidation, alkene oxidation, and oxidative naphthol coupling. At room temperature the compounds exhibit low to moderate catalytic activity in sulfoxidations and alkene oxidations, but no activity in oxidative naphthol coupling. The saturated coordination environments around the Cu centers probably are the main reason for the lower catalytic activities compared to the Ti- and V-salan analogs. Spectroscopic and mass spectrometry studies revealed that the $Cu^{II}$–salan complexes decompose, in the presence of $H_2O_2$, significantly faster at 40 °C than at room temperature. The catalytic activity observed is probably due to the $Cu^{II}$–salan degradation products, observed in the mass spectrometry studies, and not to the original $Cu^{II}$–salan precursors.



## 1. Introduction

Copper is a ubiquitous and biologically relevant metal, with $Cu^{I}$ and $Cu^{II}$ species playing relevant roles in several metabolic functions in humans [1]. Being a late transition metal, it is, in principle, capable of mediating chemical processes that are usually associated with other late transition metal analogs, such as cross-couplings [2]. In addition, copper compounds can also promote chemical processes that are associated with early transition metals such as catalytic oxidations [3].

Many authors have explored the apparent versatility of copper by developing compounds of the well-known and versatile aminophenolate class, namely of the Schiff base (SB) variant. Indeed, several authors have successfully applied Cu-(SB) catalysts in asymmetric Michael additions [4], asymmetric alkylations [5], nitroaldol reactions [6], Ulmann-type C–N cross-couplings [7], asymmetric sulfoxidations [8], alkene oxidations [9,10] and cyanohydrin synthesis [11,12].

There is one important aspect inherent to the Schiff base compounds which can impair the potential advantages offered by these Cu-(SB) catalytic systems: their hydrolytic lability. In fact, the imine moiety is prone to decomposition in the presence of water. Reduction of the C=N bond to a C–N bond yields a reduced Schiff base compound (RSB) which has higher resistance to hydrolytic decomposition and the added flexibility that a single bond provides to the overall ligand structure may enhance both activity and selectivity of the catalyst in question [13].

Studies concerning copper compounds derived from reduced salen (or "salan") ligand precursors are known [14,15], but this still remains a scarcely explored subject.

Following the previous studies of Ti-(RSB) and V-(RSB) catalytic systems carried out by our group [13], we have prepared and characterized several $Cu^{II}$ compounds bearing reduced salen (designated by salan) ligands with the goal of assessing their respective catalytic potential in various chemical transformations (Scheme 1). The compounds were tested for their catalytic activity in oxidation reactions, such as thioether and alkene oxidations, and in carbon–carbon bond formation reactions such as oxidative coupling of 2-naphthol.

## 2. Material and methods

### 2.1. Materials and equipment

Diamines cyclohexane-1,2-diamine (mixture of *trans* isomers) and (1*S*,2*S*)-1,2-diphenylethane-1,2-diamine were purchased from

* Corresponding authors.
*E-mail address:* joao.pessoa@ist.utl.pt (J.C. Pessoa).

0022-328X/$ – see front matter © 2013 Elsevier B.V. All rights reserved.
http://dx.doi.org/10.1016/j.jorganchem.2013.10.019

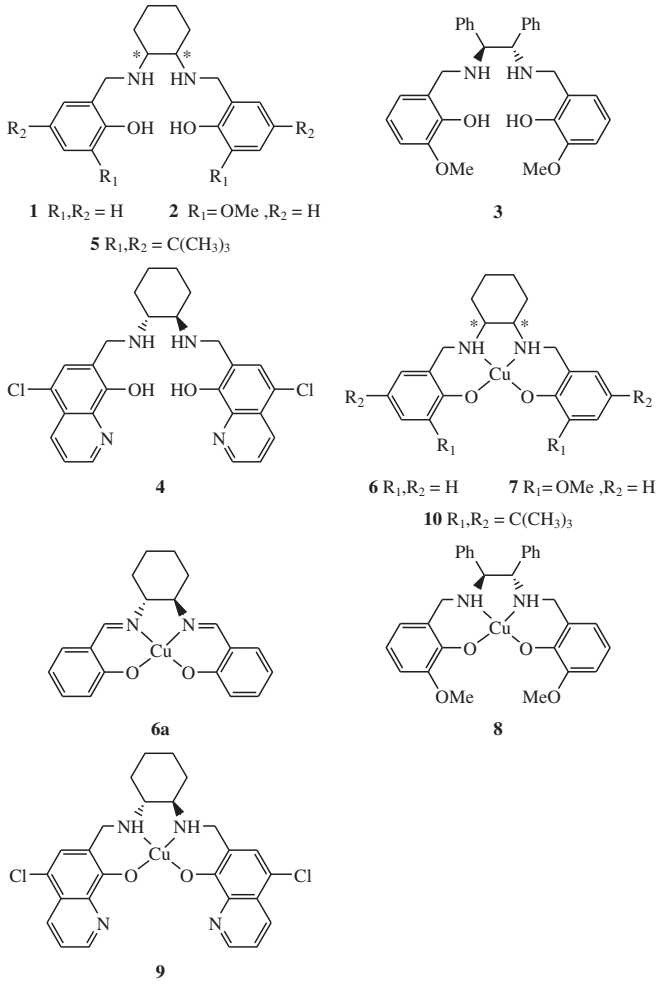


**Scheme 1.** Structural formul of the salan-type ligand precursors prepared and of the respective $Cu^{II}$ complexes.

Aldrich and Rocc, respectively. The (1*R*,2*R*) enantiomer of cyclohexane-1,2-diamine was obtained as the tartrate salt after resolution [13]. Salicylaldehyde, *o*-vanillin and 5-chloro-8-hydroxyquinoline were purchased from Aldrich. Metal precursors $Cu^{II}Cl_2$ and $Cu^{II}(OAc)_2$ monohydrate (OAc = acetate) were purchased from BDH and Panreac, respectively. Thioanisole, *trans*-anethole and 2-naphthol were purchased from Acros Organics. Hydrogen peroxide (aqueous solution, 30% w/v) was purchased from Aldrich. All chemical precursors were used as received. Solvents were purchased from Sigma–Aldrich, Carlo-Erba, Panreac and Fisher and used as received. UV–Visible spectra were recorded with a Hitachi U-2000 spectrophotometer and the Circular dichroism (CD) spectra with a Jasco J-720 spectropolarimeter. The $^{1}H$ and $^{13}C$ NMR spectra were obtained on Bruker Avance+ 400 MHz and 300 MHz Spectrometers. $^{1}H$ and $^{13}C$ chemical shifts ($\delta$) are expressed in ppm relative to $Me_4Si$ or the deuterated solvent residual peak. Elemental analyses were carried out at *Laboratório de Análises* of *Instituto Superior Técnico*, using an EA110 CE automatic analyzer Instrument. The electron paramagnetic resonance (EPR) spectra were measured with a Bruker ESP 300E X-band spectrometer, normally in frozen samples at 77 K, using DPPH radical as reference. The measured spectra (1st derivative X-band EPR) were simulated with the EPR simulation software developed by Rockenbauer and Korecz [16].

Positive ion ESI mass spectra were obtained on a 500-MS quadrupole ion trap mass spectrometer (Varian Inc., Palo Alto, CA, USA). Samples were introduced into the ESI ion source using a syringe pump set to a flow rate of 20 μL/min. The ion spray voltage was set at +5 kV; capillary voltage: 20 V and RF loading 80%. Nitrogen was used as nebulizing and drying gas, at a pressure of 25 psi and 10 psi, respectively, and the drying gas temperature was 350 °C. The spectra were recorded in the range 100–1000 Da. Spectra typically correspond to the average of 20–35 scans. Theoretical isotope patterns were calculated using the ISOPRO 3.0 program.

### 2.2. Synthesis procedures: preparation of ligand precursors

Compounds **1**, **3** and **4** were synthesized according to previously published procedures and used as their hydrochlorides [13]. Compound **2** was used as the free base. Compound **5** was prepared by adaptation of the Mannich reaction used for **4**. The respective structural formulas are shown in Scheme 1.

#### 2.2.1. Preparation procedure for *5*

The tartrate of (1*R*,2*R*)-cyclohexane-1,2-diamine (2.78 g, 10.5 mmol) was suspended in 25 mL of MeOH, and 2 equivalents of aqueous $NaHCO_3$ were added. In a separate flask, 2 equiv. of 5-chloro-8-hydroxyquinoline (3.76 g, 21.0 mmol) were dissolved in 20 mL of MeOH, and 2.5 equiv. of formaldehyde (0.79 g, 26.3 mmol, 37% aqueous solution) were added. The two solutions were mixed and refluxed for 3 h. A pale green solid formed, which was washed with water and small amounts of MeOH and diethyl ether. To decompose any 1,3-benzoxazine impurities, the solid was dissolved in ethanol and the pH was lowered to *ca.* 2. The mixture was heated to boiling point without refluxing for *ca.* 1 h. The mixture was cooled down, and after the addition of diethyl ether, a bright yellow hydrochloride precipitate was obtained which was recovered by filtration and washed with diethyl ether. Yield (hydrochloride salt): 1.86 g, 27%. $^{1}H$ NMR (300 MHz, DMSO-$d_6$, ppm): 1.19, 1.29, 1.78, 2.42 [8H, m, $-CH_2-$], 3.72 [2H, m, $CH_2CHN^+H_2$], 4.46 [2H, d, $^{2}J_{HH}$ = 13.2 Hz, Ar$-CH_2-N^+H_2$], 4.54 [2H, d, $^{2}J_{HH}$ = 13.2 Hz, Ar$-CH_2-N^+H_2$], 7.86, 8.17, 8.62, 9.03 [8H, m, aromatic]. $^{13}C$-{$^{1}H$} NMR (75 MHz, DMSO-$d_6$, ppm): $\delta$ 22.40, 25.36 [4C, $-CH_2-$], 42.42, [2C, Ar$-CH_2-N^+H_2$], 56.01 [2C, $-(CH_2)_2-CH-N^+H_2$], 116.16, 118.84, 123.99, 126.48, 130.35, 134.92, 137.01, 148.65, 151.02 [18C, aromatic]. IR ($cm^{-1}$): 3450 ($\nu$N–H), 1260 ($\nu$C–O). Elemental analysis for $C_{26}H_{30}N_4O_2Cl_6\cdot 3H_2O$: C 45.1, H 5.2, N 7.7; found: C 44.8, H 5.2, N 8.0.

### 2.3. Synthesis of $Cu^{II}$ complexes

#### 2.3.1. General preparation procedure of the $Cu^{II}$ complexes

Anhydrous $Cu^{II}Cl_2$ or $Cu^{II}(OAc)_2$ monohydrate was added to a methanolic (25 mL) solution of the appropriate ligand. After complete dissolution of the reagents, the pH was adjusted to *ca.* 7–8 with a 1 M aqueous solution of NaOH. The addition of water (25 mL) induced the complete precipitation of the desired $Cu^{II}$ compound. The resulting precipitate was filtered and washed with water and minimal amounts of diethyl ether. The recovered solid was then dried under vacuum. In the case of excessive addition of NaOH, $Cu^{II}(OH)_2$ may form. The removal of $Cu^{II}(OH)_2$ impurities can be made by dissolving the $Cu^{II}$–salan compound in dichloromethane and filtering out the inorganic impurities. The filtrate was completely evaporated in a rotary evaporator and the $Cu^{II}$–salan compound recovered. The proposed structural formulas of the $Cu^{II}$ compounds are depicted in Scheme 1.

*2.3.1.1. $Cu^{II}$[sal-(R,R-chan)], **6**.* Reagents: $Cu^{II}Cl_2$ (0.5 g, 3.7 mmol), **1** (1.5 g, 3.7 mmol). The compound was obtained as a black solid. Yield: 1.0 g, 86%. EPR (acetone/ethyleneglycol, 1:1, 77 K): $A_z$ = 189.3 × $10^{-4}$ $cm^{-1}$; $g_z$ = 2.235. Elemental analysis for $C_{20}H_{24}N_2O_2Cu\cdot 1CH_2Cl_2\cdot 0.5H_2O$: calcd. C 52.34, H 5.65, N 5.81;

found C 52.2, H 5.9, N 5.8. Crystals suitable for single crystal X-ray diffraction were grown from THF solutions: 0.1 g of **6** was dissolved in *ca.* 10 mL of THF and the resulting solution was filtered and transferred to a clean lint-free 20 mL glass flask. Dark orange crystals were obtained by slow evaporation of the solvent after approximately one week. A "half-salen" variant **6d** was obtained by dissolving 0.1 g of **6** in THF and adding 1 mol equivalent of aqueous $H_2O_2$ and leaving the solution to slowly evaporate for one week. Dark orange crystals of the **6d** were obtained.

*2.3.1.2. $Cu^{II}$[sal-(R,R-chen)],* ***6a****.* The tartrate of (1*R*,2*R*)-cyclohexane-1,2-diamine (1.35 g, 5.1 mmol) was suspended in 25 mL of MeOH, and 2 equiv of KOH (0.57 g, 10.2 mmol) in 10 mL of water were added. To this mixture 2 equiv of salicylalehyde (1.1 mL, 10.2 mmol) were added resulting in a bright yellow coloration. After stirring for 15 min, 1 equivalent of $Cu^{II}Cl_2$ (0.7 g, 5.2 mmol) dissolved in 10 mL of MeOH was added. A purple precipitate formed. The mixture was stirred vigorously for another 15 min and 80 mL of water were added. The purple solid formed was filtered and washed with water and diethyl ether. Yield: 1.7 g, 87%. EPR (THF, 77 K): $A_z = 203.2 \times 10^{-4}$ cm$^{-1}$; $g_z = 2.209$. Elemental analysis for $C_{20}H_{20}N_2O_2Cu \cdot H_2O$: calcd. C 59.77, H 5.52, N 6.97; found C 60.1, H 5.2, N 6.9. Crystals suitable for single crystal X-ray diffraction were grown from THF solutions: 0.1 g of **6a** was dissolved in *ca.* 10 mL of THF and the resulting solution was filtered and transferred to a clean lint-free 20 mL glass flask. Dark purple crystals were obtained by slow evaporation of the solvent after approximately one week.

*2.3.1.3. $Cu^{II}$[mvan-(R,R-chan)],* ***7****.* Reagents: $Cu^{II}(OAc)_2$ (0.75 g, 3.8 mmol), **2** (1.47 g, 3.8 mmol). An additional purification step was necessary due to the presence of inorganic contaminants. The crude product was extracted with 50 mL of ethanol and the mixture was filtered. The filtrate was evaporated to dryness and the resulting solid triturated with 25 mL of water. This solid was filtered and washed with water. The compound was obtained as a green solid. Yield: 0.37 g, 22%. EPR (acetone/ethyleneglycol, 1:1, 77 K): $A_z = 189.9 \times 10^{-4}$ cm$^{-1}$; $g_z = 2.237$. Elemental analysis for $C_{22}H_{28}N_2O_4Cu$: calcd. C 58.98, H 6.30, N 6.25; found C 58.7, H 6.3, N 6.2.

*2.3.1.4. $Cu^{II}$[mvan-(S,S-dpan)],* ***8****.* Reagents: $Cu^{II}Cl_2$ (0.14 g, 1.0 mmol), **3** (0.58 g, 1.0 mmol). The compound was obtained as a dark green solid. Yield: 0.32 g, 59%. EPR (acetone/ethyleneglycol, 1:1, 77 K): $A_z = 184.9 \times 10^{-4}$ cm$^{-1}$; $g_z = 2.239$. Elemental analysis for $C_{30}H_{30}N_2O_4Cu \cdot 1.8H_2O$: calcd. C 62.28, H 5.85, N 4.84; found C 62.4, H 5.6, N 4.9.

*2.3.1.5. $Cu^{II}$[5-ClQN-(R,R-chan)],* ***9****.* Reagents: $Cu^{II}Cl_2$ (0.14 g, 1.0 mmol), **4** (0.64 g, 1.0 mmol). The compound was obtained as a dark green solid. Yield: 0.34 g, 61%. EPR (DMSO/ethyleneglycol, 4:1, 77 K): $A_z = 184.9 \times 10^{-4}$ cm$^{-1}$; $g_z = 2.239$. Elemental analysis for $C_{26}H_{24}N_4O_2Cl_2Cu \cdot 1H_2O$: calcd. C 54.12, H 4.54, N 9.71; found C 54.0, H 4.6, N 10.0.

*2.3.1.6. $Cu^{II}$[3,5-di-$^t$Busal-(S,S-chan)],* ***10****.* Reagents: $Cu^{II}Cl_2$ (0.14 g, 1.0 mmol), **5** (0.6 g, 1.0 mmol). The compound was obtained as a dark green solid. Yield: 0.4 g, 66%. EPR (acetone/ethyleneglycol, 1:1, 77 K): $A_z = 184.9 \times 10^{-4}$ cm$^{-1}$; $g_z = 2.239$. Crystals suitable for single crystal X-ray diffraction were grown from isopropanol solutions: 0.1 g of **10** was dissolved in *ca.* 10 mL of isopropanol and the resulting solution was filtered and transferred to a clean lint-free 20 mL glass flask. Dark green crystals were obtained by slow evaporation of the solvent after four weeks.

### 2.4. X-ray crystal structure determination of *6*, *6a*, *6d* and *10*

The data for **6**, **6a** and **6d** were collected using graphite monochromated Mo-$K_\alpha$ radiation ($\alpha$ = 0.71073 Å) on a Bruker AXS-KAPPA APEX II diffractometer equipped with an Oxford Cryosystem open-flow nitrogen cryostat. Cell parameters were retrieved using Bruker SMART software and refined using Bruker SAINT on all observed reflections. Absorption corrections were applied using SADABS [17]. The structures were solved and refined using direct methods with programs SIR2004 [18] or SHELXS-97 [19]. All programs are included in the package of programs WINGX-Version 1.80.01 [20] SHELXL [21]. Unless stated otherwise, all non-hydrogen atoms were refined anisotropically and the hydrogen atoms were inserted in idealized positions and allowed to refine riding on the parent carbon atom. The molecular diagrams were drawn with ORTEP-3 for Windows [22] or Mercury 1.4.2 [23], included in the software package.

X-ray data for **10** were collected on a Bruker Kappa X8 Apex CCD diffractometer at 100 K. Reflections were measured from a hemisphere of data collected of frames, each covering 0.3° in $\omega$. The reflections measured were corrected for Lorentz and polarization effects, and for absorption by semi-empirical methods based on symmetry-equivalent and repeated reflections. Complex scattering factors were taken from the program package SHELXL [24]. The structures were solved by direct methods and refined by full-matrix least-squares methods on $F^2$. The non-hydrogen atoms were refined with anisotropic thermal parameters in all cases. The hydrogen atoms were left to refine freely. The crystallographic experimental data and structure refinement parameters for the above compounds are listed in Table 1.

### 2.5. Procedure for catalytic sulfoxidation of thioanisole

The catalytic experiments were carried out at atmospheric pressure at set constant temperatures in a glass batch reactor,

**Table 1**
Selected crystallographic experimental data and structure refinement parameters for **6**, **6d** and **10**.

| | **6** | **6d** | **10** |
|---|---|---|---|
| Empirical formula | $C_{40}H_{50}Cu_2N_4O_5$ | $C_{20}H_{24}CuN_2O_3$ | $C_{36}H_{56}N_2O_2Cu$ |
| Molecular weight | 793.92 | 403.95 | 612.37 |
| Temperature (K) | 150(2) | 150(2) | 100(2) |
| Crystal system | Monoclinic | Orthorhombic | Triclinic |
| Space group | $P2_1$ | $P2_12_12_1$ | P-1 |
| *a* (Å) | 7.7660(8) | 7.2160(5) | 9.9147(11) |
| *b* (Å) | 17.1000(17) | 12.1160(10) | 13.8176(17) |
| *c* (Å) | 13.7180(13) | 20.7540(16) | 14.8585(19) |
| $\alpha$ (°) | 90 | 90 | 117.610(2) |
| $\beta$ (°) | 96.369(4) | 90 | 95.249(3) |
| $\gamma$ (°) | 90 | 90 | 103.768(2) |
| *V* (Å$^3$) | 1810.5(3) | 1814.5(2) | 1703.1(4) |
| *Z*, $\rho_{calc}$ (g cm$^{-3}$) | 2, 1.456 | 4, 1.479 | 2, 1.194 |
| $\mu$ (mm$^{-1}$) | 1.225 | 1.226 | 0.673 |
| Crystal size | 0.50 × 0.40 × 0.40 | 0.40 × 0.30 × 0.08 | 0.24 × 0.07 × 0.07 |
| Crystal color | Orange | Orange | Dark green |
| Crystal shape | Block | Plate | Needle |
| Refl. collected | 22,091 | 21,751 | 13,219 |
| Unique refl. [*R*(int)] | 7290 [0.0325] | 3400 [0.0529] | 6365 [0.0444] |
| *R*1 [$I > 2\sigma(I)$][a] | 0.0290 | 0.0285 | 0.0497 |
| *wR*2 [$I > 2\sigma(I)$][b] | 0.0723 | 0.0589 | 0.1297 |
| Goodness-of-fit on $F^2$ | 1.062 | 1.048 | 1.087 |
| Absolute structure parameter | 0.022(9) | −0.007(11) | |

[a] $R_1 = \sum||F_o| - |.F_c|.|/\sum|F_o|$.

[b] $wR_2 = \{\sum[w(\left||F_o|^2 - |F_c|^2\right|)^2]/\sum[w(F_o^4)]\}^{1/2}$.

equipped with magnetic stirrer, thermometer and condenser. In a typical run, the solid catalyst and thioanisole (1.0 mmol) were dissolved in the appropriate solvent (4 mL). Then the oxidant (1.2–1.5 mmol), hydrogen peroxide (30% w/v aqueous solution) was added to the mixture. Control experiments were also carried out the in absence of catalyst.

The analysis of products of sulfoxidations was done by HPLC (Jasco system: 880-PU Intelligent HPLC Pump, a 2-line degasser 880-51, an 870-UV Intelligent UV-VIS detector) a Rheodyne 7725i injector (5 μL), using a Daicel Chiralpak IA column and a Borwin software. The eluent used was normally hexane:ethyl acetate (60:40) with a flow rate of 1 mL/min. The calibration curves for each reagent and product ($\lambda = 270$ nm), namely the sulfoxide and sulfone, were determined using similar HPLC procedures and these calibrations used for the quantitative analyses. Diphenylsulfone was used as an internal standard.

### 2.6. Procedure for catalytic oxidation of trans-anethole

The method was similar to hat used in the catalytic sulfoxidations. The solid catalyst and the alkene (1.0 mmol) were dissolved in the appropriate solvent (4 mL). Then the oxidant (2 mmol), hydrogen peroxide (30% w/v aqueous solution) was added to the stirring mixture. Control experiments were also carried out in absence of catalyst.

The analysis of products of the oxidations was done by $^1$H NMR, using either anhydrous toluene, *N*,*N*-dimethylformamide or dimethylsulfoxide as internal standards.

### 2.7. Procedure for oxidative coupling of 2-naphthol

The solid catalyst and the naphthol (1.0 mmol) were dissolved in the appropriate solvent (4 mL). The mixture was kept in contact with air during the catalytic run. Control experiments were also carried out in absence of catalyst.

The analysis of products of the oxidations was done by HPLC using the equipment described in the procedure for catalytic sulfoxidations. The eluent used was normally hexane: 1-propanol (90:10) with a flow rate of 1 mL/min. The calibration curve for the product ($\lambda = 254$ nm), the binaphthol, was determined using similar HPLC procedures and these calibrations used for the quantitative analyses. Acetophenone was used as internal standard.

## 3. Results and discussion

### 3.1. Synthesis and characterization of the $Cu^{II}$ complexes

Five $Cu^{II}$–salan compounds were prepared by adapting a reported procedure [13] which employed a $Cu^{II}$ precursor such as anhydrous $Cu^{II}Cl_2$ or $Cu^{II}(OAc)_2$ monohydrate and an appropriate salan-type ligand. All $Cu^{II}$–salan compounds presented as green to dark green solids which are soluble in polar organic solvents. Characterization was made by X-band continuous wave electron paramagnetic resonance (EPR), circular dichroism (CD), electronic absorption spectroscopy (UV–Vis) and also by elemental analysis. Suitable crystals for single-crystal X-ray diffraction were obtained for compounds **6**, **6a** and **10**. Study of the interactions of **6** with $H_2O_2$ by UV–Vis and CD was also attempted. In addition, it was possible to obtain crystals of the product resultant from the interaction of **6** with $H_2O_2$, which was revealed by crystal X-ray diffraction to be the "half-salen" variant of **6**, which will be referred to as **6d**. A more detailed discussion of the results is made in the following sections.

#### 3.1.1. X-ray diffraction studies

ORTEP diagrams of **6** (molecule ***b***), **6d** and **10** are depicted in Figs. 1, 3 and 4, respectively. Selected bond lengths and angles for the compounds are listed in Table 2.

Compound **6** (see Figs. 1 and 2) crystallized in the monoclinic system, space group $P2_1$, with the unit cell containing two molecules having different spatial arrangement (**6*b*** and **6*c***, Fig. 2) in the asymmetric unit. Both molecules present square-planar coordination around the Cu center as predicted earlier by EPR spectroscopy, with the equatorial planes defined by atoms O1, O2, N1 and N2. The main difference between the two molecules relies in the distortion of the square-planar geometry of the metal center. In one of the molecules, **6*b***, the distortion is minimal with atoms O1, O2, N1 and N2 deviating 0.035(1), 0.035(1), 0.033(1), 0.033(1) Å from the equatorial mean square plane. In the other molecule, **6*c***, there is a higher distortion of the square planar geometry with atoms O1, O2, N1 and N2 deviating 0.225(1), 0.224(1), 0.216(1), 0.214(1) Å from the equatorial mean square plane. The different coordination geometry in molecules **6*b*** and **6*c*** is illustrated in Fig. 2.

In **6*b*** the $Cu^{II}$-donor atom bond distances do not differ much and the bond angles between the *cis* $Cu^{II}$–$O_{phenolate}$ and the $Cu^{II}$–$N_{amine}$ bonds are approximate to 90°. Further attesting the square-planar geometry are the *trans* $Cu^{II}$–$O_{phenolate}$ and the $Cu^{II}$–$N_{amine}$ bond angles with values very approximate to 180°. The overall bond lengths are very similar to those reported in the literature for structurally related square-planar $Cu^{II}$–salan compounds [25]. In **6*c***, the distortion of the square planar geometry is more pronounced in the *trans* $Cu^{II}$–$O_{phenolate}$ and the $Cu^{II}$–$N_{amine}$ bond angles (about 167°) which deviate significantly from 180°. These angles are similar to those found in the distorted structure of the Schiff base version reported earlier by Cross and co-workers [8].

**6*a*** crystallized in the monoclinic system, space group $P2_1$, with two molecules of (*R*,*R*)-**6*a*** in the asymmetric unit. The crystallographic (see ESI) data are in agreement with those previously reported by Meunier and co-workers [26].

Compound **6*d***, a half-salen version of **6**, crystallized in the orthorhombic system, space group $P2_12_12_1$, with one molecule in the unit cell (Fig. 3). This is the first structure of a half-salen based on a chiral cyclohexene-1,2-diamine scaffold reported so far. The only example of a half-salen based on ethylenediamine (non-chiral), reported by Reglinski and co-workers, was obtained by oxidative dehydrogenation of the corresponding salan complex [27]. The geometry around the Cu center is once again square planar with atoms O1, O2, N1 and N2 defining the equatorial plane. The C7–N1 bond length is, as expected, shorter than in **6** (1.281(3) Å versus 1.491(4)). The C7–N1–Cu1 angle is also wider in

**Table 2**
Selected bond lengths (Å) and angles (°) for compounds **6**, **6d** and **10**.

| | **6** | | **6d** | **10** |
|---|---|---|---|---|
| | ***b*** | ***c*** | | |
| Cu(1)–N(1) | 1.996(2) | 1.993(3) | 1.926(2) | 1.9919(2) |
| Cu(1)–N(2) | 1.984(2) | 2.003(2) | 1.999(2) | 1.9927(2) |
| Cu(1)–O(1) | 1.8940(19) | 1.885(2) | 1.9134(16) | 1.8946(2) |
| Cu(1)–O(2) | 1.895(2) | 1.905(2) | 1.8916(16) | 1.8870(2) |
| C(7)–N(1) | 1.491(4) | 1.483(4) | 1.281(3) | 1.4707(2) |
| C(14)–N(2) | 1.486(4) | 1.488(3) | 1.464(3) | 1.4744(1) |
| O(1)–Cu(1)–O(2) | 85.09(9) | 87.88(11) | 87.75(7) | 88.33(11) |
| O(1)–Cu(1)–N(1) | 95.01(9) | 94.45(10) | 94.10(8) | 92.79(12) |
| O(2)–Cu(1)–N(2) | 93.29(8) | 94.19(8) | 94.18(8) | 92.86(12) |
| N(1)–Cu(1)–N(2) | 86.66(10) | 86.39(11) | 85.39(9) | 86.05(13) |
| C(7)–N(1)–Cu(1) | 110.92(19) | 112.0(2) | 125.39(18) | 111.0(2) |
| C(14)–N(2)–Cu(1) | 110.00(17) | 111.81(18) | 110.93(17) | 110.5(2) |
| O(1)–Cu(1)–N(2) | 176.45(9) | 167.80(10) | 170.46(9) | 177.84(12) |
| O(2)–Cu(1)–N(1) | 179.10(9) | 166.22(10) | 171.29(9) | 178.47(13) |

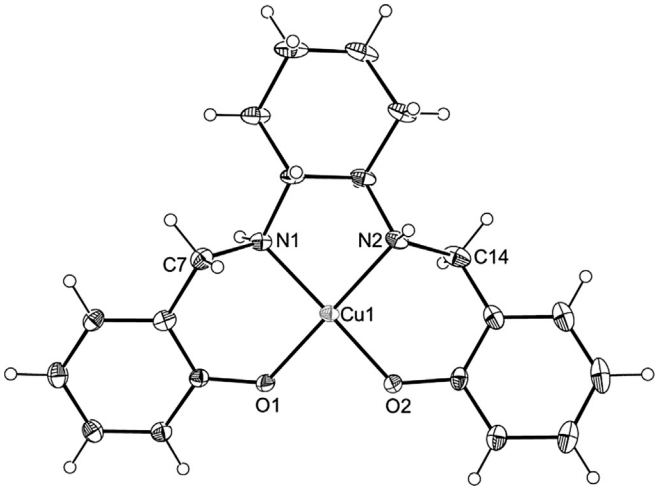


**Fig. 1.** ORTEP-3 diagram of **6**, molecule ***b***, using 30% probability level ellipsoids.

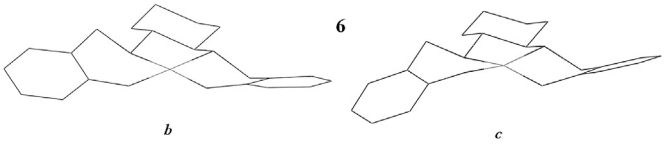


**Fig. 2.** Diagram, drawn by Mercury software, illustrating the difference in the distortion of the square planar coordination geometry in the two molecules of **6** (**6*b*** and **6*c***).

**6*d*** than in **6** (125.39(18) versus 110.92(19) °). These values are in accordance with those observed for Reglinski's half-salen [27].

The structure obtained for **10** (Fig. 4) also exhibits a $Cu^{II}$ center in a square-planar environment. The overall bond distances and angles are very similar to those found in **6** and are in agreement with those reported in the literature for other square-planar $Cu^{II}$–salan complexes [25]. This compound crystallized in the triclinic system, space group P-1, a centrosymmetric space group. This indicates that a racemic mixture is present in the crystal, possibly as a result of an incomplete resolution of the precursor diamine. As such, 50% of the molecules present in the crystal structure have *R* configuration at C(8) and C(13) and *S* configuration at the nitrogen donors N(1) and N(2). The other 50% have opposite configurations at these atoms.

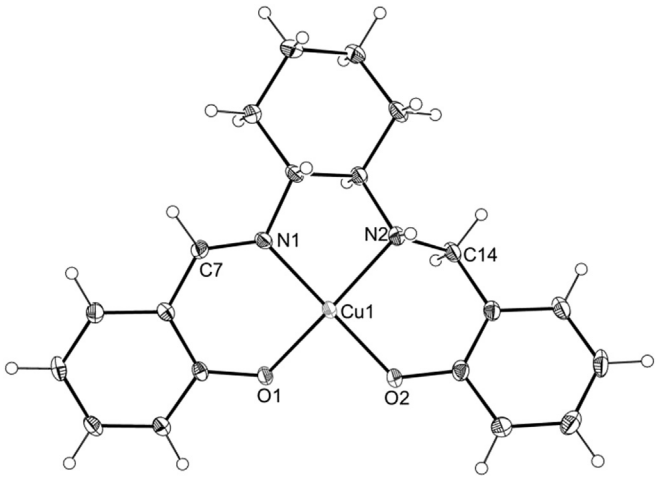


**Fig. 3.** ORTEP-3 diagram of **6d**, using 30% probability level ellipsoids.

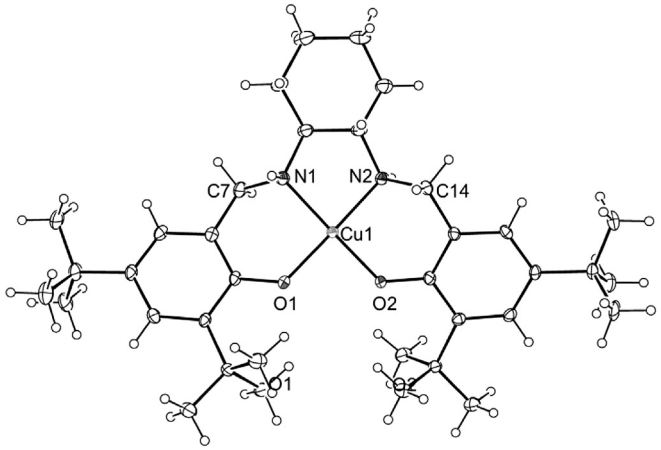


**Fig. 4.** ORTEP-3 diagram of **10**, using 30% probability level ellipsoids.

### 3.1.2. EPR spectroscopy

As $Cu^{II}$ is a $3d^9$ metal ion, with a nuclear spin of $I = 3/2$, it is suitable for characterization by X-band EPR. Due to the broadened signals and the variability introduced by any possible tetrahedral distortion, $Cu^{II}$ EPR normally does not allow an accurate distinction between the various types of donor atoms. Namely, it may not be possible to distinguish between an aliphatic N-amine donor and an *N*-pyridine-type donor. Nevertheless, the Peisach–Blumberg $A_{||}$ and $g_{||}$ correlation plots and the tetrahedral distortion index $g_z/A_z$ reported by Addison and co-workers [28] have been used to interpret the experimental *z*-component parameters.

In Fig. 5 are depicted the 1st derivatives of the EPR spectra of the featured $Cu^{II}$–salan compounds; the corresponding spin Hamiltonian parameters are listed in Table 3.

The $Cu^{II}$–salan compounds exhibit $A_z$ and $g_z$ values consistent with mixed [N,O] binding sets and essentially square-planar geometry. The $g_z/A_z$ ratios are within the 100–135 cm range expected for square-planar $Cu^{II}$ species with minimal tetrahedral distortion. Comparison of these data with spin Hamiltonian parameters reported by other authors [10,29a–h] for closely related $Cu^{II}$–salen and $Cu^{II}$–salan compounds was also made.

In the case of **9**, there are four nitrogen donors but it is not possible to determine if the $Cu^{II}$ center is coordinated to the aliphatic amine or pyridine donors. Nevertheless, by comparison with literature reports, the spin Hamiltonian parameters obtained

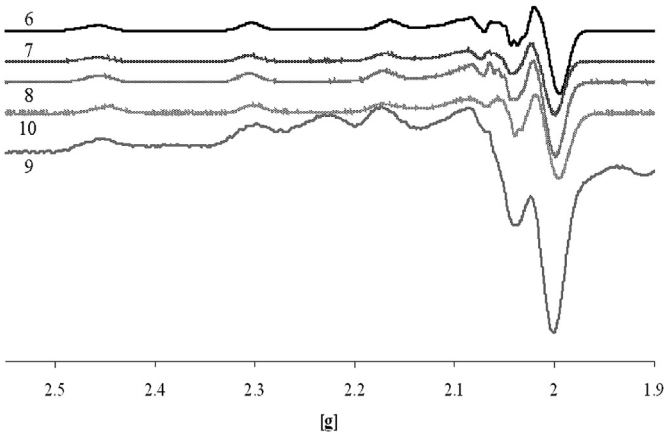


**Fig. 5.** First derivatives of the X-band EPR spectra of the $Cu^{II}$–salan compounds **6**, **7**, **8**, **9** and **10**, measured at 77 K.

**Table 3**
Experimental spin Hamiltonian parameters for the prepared $Cu^{II}$–salan compounds.[a]

| Compound | $g_x$, $g_y$ | $A_x$, $A_y$ | $g_z$ | $A_z$ | $g_z/A_z$ |
|---|---|---|---|---|---|
| | | $\times 10^4$ cm$^{-1}$ | | $\times 10^4$ cm$^{-1}$ | cm |
| **6** | 2.038, 2.057 | 36.4, 10.6 | 2.235 | 189.3 | 118 |
| **7** | 2.057, 2.033 | 26.4, 18.5 | 2.237 | 189.9 | 118 |
| **8** | 2.037, 2.055 | 28.3, 22.5 | 2.239 | 184.9 | 121 |
| **9**[b] | 2.048 | 18 | 2.239 | 184.9 | 121 |
| **10** | 2.038, 2.056 | 36.1, 7.8 | 2.238 | 184.9 | 121 |

[a] EPR spectra measured at 77 K with a 1:1 acetone:ethyleneglycol mixture as solvent.
[b] EPR spectrum measured at 77 K with a 4:1 DMSO:ethyleneglycol mixture as solvent.

for the compounds presented herein are consistent with a $[N_2,O_2]$ binding set. An additional feature observed in the spectra of compounds **6** and **8** is the existence superhyperfine $^{14}N$ splittings [30] in the high-field regions (See Figs. SI-1 and SI-2 in the Supplementary data). The $a_{\perp}^{N}$ superhyperfine coupling constant was estimated for both **6** and **8** and the obtained value of *ca.* $12 \times 10^{-4}$ cm$^{-1}$ is close to those reported for other $Cu^{II}$–salan compounds [29d]. The superhyperfine structures observed in both cases are indicative of coupling of the electronic spin with two equivalent $^{14}N$ nuclei ($2 \times 2 \times 1 + 1 = 5$ splittings).

### 3.1.3. Electronic absorption and CD spectroscopy

The recorded electronic absorption and CD spectra for the $Cu^{II}$–salan compounds in solution are depicted in Figs. 6 and 7 and the respective $\lambda_{max}$, $\varepsilon$ and $\Delta\varepsilon$ values are listed in Tables 4 and 5. Compounds **6**, **7**, **8** and **10** exhibited a broad band at *ca.* 580 nm assigned to an envelope of *d*–*d* transitions partially allowed in a non-centrosymmetric square-planar $Cu^{II}$ complex; hence the $\varepsilon$ values over 200 M$^{-1}$ cm$^{-1}$ in most cases [31]. The exception is compound **9** which shows no apparent bands within the 900–500 nm range, although it is very likely that the expected *d*–*d* transitions are masked by the very broad and intense charge transfer bands. The more intense bands centered at *ca.* 400 nm are assigned to the $Cu^{II}$–$O_{phenolate}$ ligand-to-metal charge transfer transitions and also to the $n$–$\pi$ imine transitions in the case of **6a**; the bands below 330 nm are assigned to intraligand transitions.

The CD spectra of the above compounds (Fig. 7) show optical activity associated with the *d*–*d* transitions at *ca.* 580 nm, which in turn may be indicative of chirality at the metal center. Compound **9** shows only very weak optical activity in this range, but reveals the *d*–*d* transitions which were not clearly observable in the corresponding electronic absorption spectrum. This observation may also provide an answer not given by the EPR characterization of this compound: the $Cu^{II}$ center may be coordinated by the N-pyridine donors instead of the aliphatic N-amine donors. The increased distance from the carbon stereocenters thus results in very low optical activity associated with any observable *d*–*d* transitions.

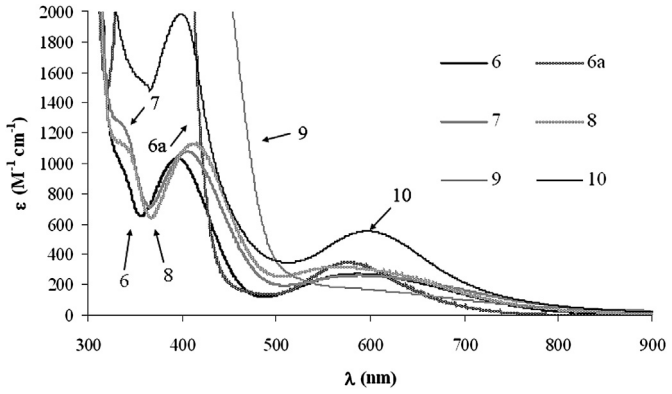


**Fig. 6.** Isotropic electronic absorption spectra of **6** (THF, 1.14 mM), **6a** (THF, 1.23 mM), **7** (THF, 1.01 mM), **8** (THF, 0.20 mM), **9** (DMF, 0.86 mM) and **10** (THF, 0.97 mM) recorded at room temperature, with 1 cm optical path.

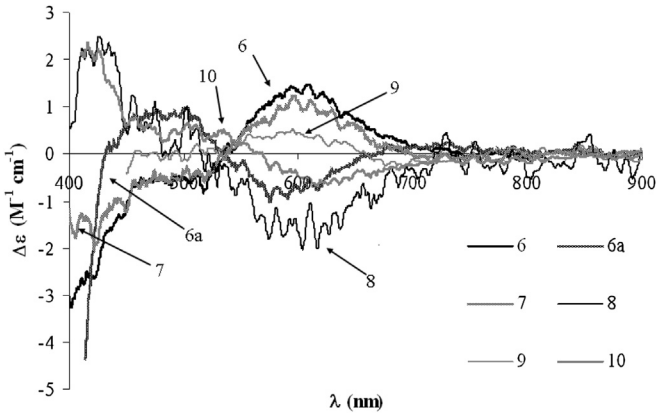


**Fig. 7.** Circular dichroism (CD) spectra of **6** (THF, 1.14 mM), **6a** (THF, 1.23 mM), **7** (THF, 1.01 mM), **8** (THF, 0.20 mM), **9** (DMF, 0.86 mM) and **10** (THF, 0.97 mM) recorded at room temperature, with 5 mm optical path.

It is also worth noting that in the 900–450 nm region the spectra of the salan and salen compounds **6** and **6a** are nearly mirror images, despite both complexes having the same configuration at the stereogenic carbons. The chirality at the metal center depends greatly on its immediate vicinity. In this case, the distinct $sp^3$ and $sp^2$ nitrogen donor atoms of the ligand structures impart very distinct optical activity at the $Cu^{II}$ center.

All compounds, with the exception of **9** due to too high absorption of the sample, not allowing the measurement of the CD spectra in adequate conditions, exhibit optical activity associated with the charge transfer transitions at *ca.* 400 nm.

## 3.2. Catalytic applications of the $Cu^{II}$–salan complexes

### 3.2.1. Sulfoxidation of thioanisole

The featured $Cu^{II}$–salan compounds were screened for their catalytic potential in the asymmetric sulfoxidation of thioanisole under a variety of conditions, using aqueous $H_2O_2$ as oxidant. The more relevant results obtained are listed in Table 6. In the Supporting information a more complete set of the results obtained is included (Table SI-1). Of the $Cu^{II}$–salan compounds tested, only compounds **6** and **7** exhibited moderate to low catalytic activity and very low enantioselectivity under the conditions listed in Table 6. In

**Table 4**
Experimental $\lambda_{max}$, $\varepsilon$ and $\Delta\varepsilon$ values obtained in the visible range for compounds **6**, **6a**, **7**, **8**, **9** and **10**.

| Isotropic absorption spectra (UV–Vis) | | | | | |
|---|---|---|---|---|---|
| $\lambda$ (nm) | $\varepsilon$ (M$^{-1}$ cm$^{-1}$) | $\lambda$ (nm) | $\varepsilon$ (M$^{-1}$ cm$^{-1}$) | $\lambda$ (nm) | $\varepsilon$ (M$^{-1}$ cm$^{-1}$) |
| **6** | | **6a** | | **7** | |
| 587 | 270 | 577 | 346 | 589 | 262 |
| 395 | 1033 | | | 406 | 1079 |
| **8** | | **9**[a] | | **10** | |
| 565 | 318 | – | – | 598 | 554 |
| 413 | 1128 | – | – | 399 | 1986 |

[a] No bands were identified in the visible range due to masking by the charge-transfer bands.

**Table 5**
Experimental $\lambda_{max}$, $\Delta\varepsilon$ values obtained in the visible range for compounds **6**, **6a**, **7**, **8**, **9** and **10**.[a]

| Circular dichroism (CD) | | | | | |
|---|---|---|---|---|---|
| $\lambda$ (nm) | $\Delta\varepsilon$ ($M^{-1}$ $cm^{-1}$) | $\lambda$ (nm) | $\Delta\varepsilon$ ($M^{-1}$ $cm^{-1}$) | $\lambda$ (nm) | $\Delta\varepsilon$ ($M^{-1}$ $cm^{-1}$) |
| **6** | | **6a** | | **7** | |
| 594 | 1.42 | 576 | −1.02 | 611 | 1.12 |
| | | 503 | 0.98 | | |
| **8** | | **9** | | **10** | |
| 604 | −2.02 | 710 | −0.21 | 616 | −0.67 |
| | | 595 | 0.52 | | |

[a] Absorption maximum of bands below 450 nm were not identified due to too high absorption of the samples, thus yielding a too high signal-to-noise ratio of the CD spectra.

general, the selectivity towards the formation of the sulfoxide product appears largely insensitive to the solvent and temperature parameters, as sulfone yields do not exceed 1% in the cases where a significant conversion was observed. In addition, the sulfoxidation appears to proceed faster in methanol than in the 3:1 acetone:-water mixture (entries 2 and 5). In the case of **6**, the use of acetic acid as an additive had little or no effect on overall yields and enantiomeric excesses (see Table SI-1 entries 2, 5, 6, 8 and 10).

Temperature had only an effect on yields, with lower temperatures greatly extending the reaction time necessary to obtain yields comparable to those obtained in methanol at 40 °C with acetic acid additive, which did not exceed 52% (entries 1–6). Compound **7** was used only in mild conditions with the expectation that the methoxy groups of the phenolate moieties would improve activity and enantioselectivity, similarly to what was reported with V-salan analogs [13]. However, only very low conversions and enantiomeric excesses were observed (entries 7 and 8). Compounds **8**, **9** and **10** exhibit catalytic activity and enantioselectivity comparable to that observed with **6** in methanol (entries 10, 12 and 14). Compounds **8** and **9**, however, exhibited low activities in acetone/water mixture (entries 9 and 11). In contrast, **10** performed better in acetone/water mixture (entry 13), giving a conversion comparable to those obtained with **6**, **8** and **9** in methanol.

In terms of activity and enantioselectivity, the $Cu^{II}$–salan compounds presented herein contrast sharply with $Ti^{IV}$ and $V^{IV}O$ compounds using the same ligand support, but still perform better than $Cu^{II}(OAc)_2$ under the same conditions (see Table SI-1 entries 21 and 22) [13]. The reasons behind the low catalytic activity of these $Cu^{II}$–salan compounds in sulfoxidation may be due to the saturated coordination sphere of the $Cu^{II}$ center, which makes the $Cu^{II}$–salan complex unable to accommodate and activate the oxidant, thus not generating the electrophilic copper-peroxido/hydroperoxido species which is thought to be crucial in the S-oxidation processes mediated by the vanadium counterparts [32].

**Table 6**
Results obtained from $Cu^{II}$–salan catalyzed thioanisole sulfoxidation.[a]

| Entry | Compound | Solvent | $T$ (°C) | Conversion (%)[b] | Sulfoxide (%)[b] | Sulfone (%)[b] | ee (%)[b] |
|---|---|---|---|---|---|---|---|
| 1 | **6** | Acetone/$H_2O$ (3:1) | 0 | 3[c] | 2 | 1 | 3 |
| 2 | **6** | Acetone/$H_2O$ (3:1) | 25 | 13 | 12 | 1 | 0 |
| 3 | **6** | Acetone/$H_2O$ (3:1) | 40 | 45 | 45 | <1 | 1 |
| 4 | **6** | Methanol | 0 | 46[c] | 45 | 1 | 2 |
| 5 | **6** | Methanol | 25 | 33 | 33 | 0 | 2 |
| 6 | **6** | Methanol | 40 | 52[d] | 52 | <1 | 1 |
| 7 | **7** | Acetone/$H_2O$ (3:1) | 25 | 8 | 8 | <1 | 3 |
| 8 | **7** | Acetone/$H_2O$ (3:1) | 25 | 11[d] | 11 | <1 | 2 |
| 9 | **8** | Acetone/$H_2O$ (3:1) | 25 | 8 | 8 | 0 | 2 |
| 10 | **8** | Methanol | 25 | 32 | 37 | 0 | 0 |
| 11 | **9** | Acetone/$H_2O$ (3:1) | 25 | 0[d] | | | |
| 12 | **9** | Methanol | 25 | 36 | 36 | 0 | 0 |
| 13 | **10** | Acetone/$H_2O$ (3:1) | 25 | 34 | 34 | 0 | 2 |
| 14 | **10** | Methanol | 25 | 21 | 21 | 0 | 2 |

[a] Unless stated otherwise, the reaction conditions were the following: 1 mmol of thioanisole, 1 mol% of $Cu^{II}$ compound, 4 mL of solvent, single addition of oxidant (1.2 mmol). The reaction mixture stirred for 24 h at the set temperature.
[b] Conversion, product percentages and enantiomeric excesses were determined by chiral HPLC. Product percentages are presented as relative to the maximum quantity obtainable for each product under these conditions (1 mmol).
[c] Conversion after 72 h.
[d] Addition of 10 mol% of acetic acid.

### 3.2.2. Oxidation of trans-anethole

The $Cu^{II}$–salan compounds **6**, **7** and **9** were tested for their catalytic activity in alkene oxidation under a variety of conditions, also using aqueous $H_2O_2$ as oxidant. Naturally occurring *trans*-anethole was chosen as substrate due to its relatively low cost and ease of handling compared to other common alkene substrates such as styrene. Being *trans*-anethole an electron-rich alkene, we anticipate it to be particularly susceptible to oxidation at the carbon–carbon double bond by electrophilic peroxido species. However, the epoxide product is known to be highly reactive and easily undergoes oxidative cleaving, generating *p*-anisaldehyde and *p*-anisic acid as by-products, along with other epoxide ring-opening by-products [33]. Scheme 2 shows the possible outcomes in the $Cu^{II}$–salan catalyzed oxidation of *trans*-anethole with aqueous $H_2O_2$. The more relevant results obtained are listed in Table 7. In the Supporting information a more complete set of the results obtained is included (Table SI-2).

Several control reactions without the catalyst were carried out in methanol and acetone/water 3:1 mixture using 2 mole equivalents of $H_2O_2$. No oxidation reaction was observed after 72 h at room temperature with both solvents. Addition of 10 mol% of acetic acid did not promote substrate oxidation in methanol without the $Cu^{II}$ catalyst after 72 h at room temperature. Control reactions at 40 °C also showed that there is little oxidation of anethole. For instance, when using acetonitrile or acetone/water 3:1, with 10 mol % of acetic acid, anethole oxidation did not go beyond 9% after 24 h. Using methanol as solvent at 40 °C without any additive resulted in the oxidation of 19% of the starting material (to get 2% of *p*-anisaldehyde, 9% of epoxide ring opening product and 8% of non-identified products) after 24 h, while in acetone/water 3:1 there was no conversion of anethole.

When employing the $Cu^{II}$–salan compounds as catalyst precursors, the conversions achieved were moderate, with the product outcomes being dependent on the solvent used. In addition, the presence of a protic co-solvent or additive was necessary for the oxidations to proceed. For instance, when the reaction was carried out with **6** in acetone there was no conversion at 25 °C, while the addition of 10 mol% of acetic acid under the same conditions allowed the conversion of 37% of the alkene, with 57% of the

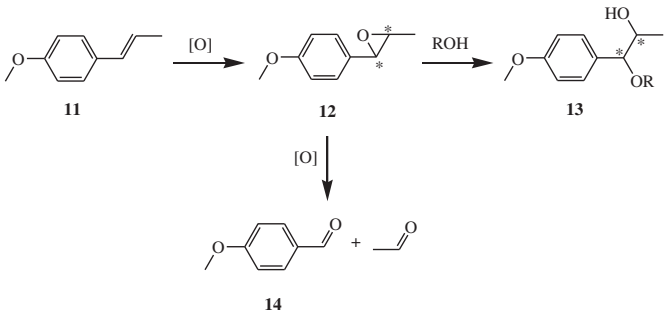


**Scheme 2.** Some of the possible oxidation products of *trans*-anethole. The asterisk (*) indicates a stereogenic carbon atom.

**Table 7**
Results obtained from $Cu^{II}$–salan catalyzed *trans*-anethole oxidation.[a]

| Entry | Compound | Solvent | $T$ (°C) | Conv. (%)[b] | Products selectivity and diastereoselectivity[b] | | | | | |
|---|---|---|---|---|---|---|---|---|---|---|
| | | | | | **12** (%) | **13** (%) | **14** (%) | Other (%) | de (**12**) (%) | de (**13**) (%) |
| 1 | **6** | Acetone | 25 | 0 | | | | | | |
| 2 | **6** | Acetone | 25 | 37[c] | 57 | | 43 | | 33 (*cis*) | |
| 3 | **6** | Acetone/$H_2O$ (3:1) | 40 | 60 | 59 | | 38 | 3 | 36 (*cis*) | |
| 4 | **6** | Acetone/$H_2O$ (3:1) | 40 | 59 | 42 | | 32 | 26 | 39 (*cis*) | |
| 5 | **6** | Methanol | 40 | 37 | | 49 | 16 | 35 | | 18 (*u*) |
| 6 | **7** | Acetone/$H_2O$ (3:1) | 40 | 53 | 40 | | 34 | 26 | 40 (*cis*) | |
| 7 | **7** | Methanol | 40 | 63 | | 43 | 24 | 33 | | 14 (*u*) |
| 8 | **9** | Acetone/$H_2O$ (3:1) | 25 | 0 | | | | | | |
| 9 | $Cu^{II}(OAc)_2$ | Acetone/$H_2O$ (3:1) | 40 | 37 | 19 | | 49 | 32 | 43 (*cis*) | |
| 10 | $Cu^{II}(OAc)_2$ | Methanol | 40 | 24 | | 25 | 38 | 37 | | 33(*u*) |

[a] Unless stated otherwise, the reaction conditions were the following: 1 mmol of *trans*-anethole, 1 mol% of catalyst, 4 mL of solvent, single addition of $H_2O_2$ (2 mmol). The reaction mixture stirred for 24 h at the set temperature.
[b] Conversion, product selectivities and diastereoselectivities were determined by $^1H$ NMR.
[c] Addition of 10 mol% of acetic acid.

generated products being the epoxide (entries 1 and 2). Water was then included as a protic co-solvent by employing 3:1 acetone/water mixtures. There was no reaction at 0 °C and 25 °C (see Table SI-2 entries 3 and 4), and it was observed that the highest conversions were only obtained at 40 °C, after 24 h (entries 3 and 4). Acid and basic additives were also tested, but the result was either the inhibition of the oxidation with $Na_2CO_3$ as an additive, or the lowering of conversion and epoxide percentages when acetic acid was used instead (see Table SI-2 entries 5, 8 and 10). Using $NH_4Cl$ as an additive resulted in a significant formation of *p*-anisaldehyde along with other products which could not be identified by $^1H$ NMR (see Table SI-2 entry 9). When solvents such as acetonitrile, chloroform and isopropanol were used, no alkene oxidation was observed (see Table SI-2 entries 11, 12 and 13). Remarkably, using methanol as solvent favored the epoxide ring-opening pathway. The amounts of *p*-anisaldehyde formed are effectively lowered to half of those observed in acetone/water mixtures and the main product is 1-methoxy-1-(4-methoxyphenyl)propan-2-ol [33], although a significant amount of non-identified by-products was still present (entry 5).

In methanol the oxidations occurred only at 40 °C. The addition of acetic acid resulted in a slight increase of *p*-anisaldehyde formation, while $Na_2CO_3$ inhibited the oxidation reaction entirely (see Table SI-2 entries 17 and 18). With compound **7**, the catalyst activity and selectivity in acetone/water and methanol (entries 6 and 7) was very similar to that observed with **6**. Compound **9** did not promote the oxidation under the conditions tested, most likely due to its insolubility in the acetone/water solvent mixture (entry 8). Nevertheless, the tested $Cu^{II}$–salan compounds proved to be better than $Cu^{II}(OAc)_2$ under the same conditions in terms of activity and product selectivity (entries 9 and 10). More specifically, the $Cu^{II}$–salan compounds favored the formation of the epoxide or 1-methoxy-1-(4-methoxyphenyl)propan-2-ol at 40 °C, while $Cu^{II}(OAc)_2$ favored mainly the formation of *p*-anisaldehyde and other non-identified oxidation by-products. In terms of diastereoselectivity, there was no apparent advantage from using $Cu^{II}$–salan catalysts over $Cu^{II}(OAc)_2$ in acetone/water at 40 °C as the diastereoisomeric excess obtained was *ca.* 40% of *cis* product in these instances. Compounds **6** and **7** showed a higher preference for the formation of *like* products in methanol at 40 °C than $Cu^{II}(OAc)_2$, as shown by the lower diastereoselectivities of **6** and **7** of *ca.* 18% *unlike* product versus 33% observed for $Cu^{II}(OAc)_2$.

A question remains as to the product profiles obtained in methanol. The observation of 1-methoxy-1-(4-methoxyphenyl) propan-2-ol as a final product implies the formation of the reactive anethole epoxide as an intermediate which then undergoes a ring-opening reaction with methanol as the nucleophile. The question resides in the likelihood of this process being metal-catalyzed and to what extent. While there are reports of $Cu^{II}$-catalyzed epoxide ring-opening [34], it must be also considered that the reaction temperature of 40 °C may also facilitate the non-catalyzed $Sn_2$ reaction between the reactive epoxide and methanol. Thus, the extent of the $Cu^{II}$–salan catalyzed anethole epoxide ring-opening reaction cannot be unambiguously determined using the present information. Another noteworthy aspect is the overall prevalence of the *cis* epoxide, which indicates that the oxidation process proceeds mostly by a stepwise oxidation mechanism, possibly of radicalar nature [35]. If the main oxidation pathway was a concerted mechanism, the majority of the epoxide obtained would be *trans*. The lower diastereoselectivities of the ring-opening products may be explained by the preferential consumption of the *cis* epoxide ((2*R*,3*S*)-2-(4-methoxyphenyl)-3-methyloxirane) to yield a *like* product ((1*S*,2*S*)-1-methoxy-1-(4-methoxyphenyl)propan-2-ol), considering the inversion of configuration at the benzylic carbon of the epoxide upon attack of the nucleophile.

### 3.2.3. Oxidative coupling of 2-naphthol

Compound **6** was tested for its catalytic potential in the oxidative coupling of 2-naphthol to yield 1,1′-bi-2-naphthol (BINOL) under mild aerobic conditions. However, despite of the extended reaction times, elevated temperatures and use of additives, no reaction was observed in the seven catalytic runs carried out. Because the copper-mediated oxidative coupling of phenols is thought to involve coordination of the substrate and reduction of the metal center, the saturated coordination sphere and the highly stabilized +2 oxidation state of copper centers may be the reason for the non-activity of the salan compounds tested [36–40]. The obtained results are included as Supplementary data (See Table SI-3).

## 3.3. Study of the interaction of **6** with $H_2O_2$

Similarly to previous studies regarding the interaction of metal–aminophenolate class compounds with hydrogen peroxide [13,–k], the behavior of the model compound **6** in the presence of an excess of this oxidant was monitored by electronic absorption and CD techniques and also by electrospray ionization mass spectrometry (ESI-MS).

The first part of this study was carried out by adding 10 mol equivalents of $H_2O_2$ to a solution of **6** in THF and observing the changes occurred after a 24 h period at room temperature. The result was an increase of overall band intensity and a slight shift to the $\lambda_{max}$ versus a control sample with similar concentration, such

that a profile identical to **6a** was obtained (Fig. 8). An additional experiment at 40 °C was carried out using another solution of **6** in THF. The determination of $\varepsilon$ values in this case was not possible due to the formation of a small amount of a precipitate which was removed using a syringe microfilter. Nevertheless, Fig. 8 shows the obtained spectrum in comparison with those obtained for **6** and **6a**. The spectrum obtained at 40 °C in the presence of $H_2O_2$ is similar to that obtained at room temperature, albeit with broadening and slight blue-shift of the *d*–*d* transition at *ca*. 570 nm. The CD spectra obtained from these solutions also show noticeable changes (Fig. 9). Again, due to the formation of a very fine precipitate in the solution subject to 40 °C, comparison between $\Delta\varepsilon$ values cannot be made.

An explanation for these spectral changes is the conversion of the $Cu^{II}$–salan compound into a $Cu^{II}$–salen species by oxidative dehydrogenation of the ligand [27]. This could explain the similarity between the electronic absorption spectra of **6a** and **6**/$H_2O_2$ and the decreased optical activity in the 900–400 nm range, considering that **6** and **6a** have near mirror image profiles in this range. Once the salen species is formed, degradation by hydrolysis of the C=N bonds may then ensue, further changing the electronic absorption and CD profiles.

The positive-ion ESI mass spectra provide further evidence supporting the occurrence of oxidative dehydrogenation of the ligand. The proposed structural formulas and masses for **6**, **6a**, **6d** and the respective degradation products are included as Supplementary data (Fig. SI3). Spectra of **6** and **6a** in the absence of oxidant were recorded for control (Fig. 10). The mass spectrum of **6** shows groups of peaks at *m*/*z* 775/777 (base peak) and 797/799 attributed to the protonated dimer $[(\mathbf{6})_2H]^+$ and its sodium adduct $[(\mathbf{6})_2Na]^+$, respectively. The peaks at *m*/*z* 388 and 410 were assigned to the protonated molecule $[\mathbf{6}H]^+$ and its sodium adduct $[\mathbf{6}Na]^+$, respectively. Compound **6a** presented two major group of peaks at *m*/*z* 406 and 789/791 (inset in the spectrum of **6a**, Fig. 10) corresponding to the sodium adducts $[\mathbf{6a}Na]^+$ and $[(\mathbf{6a})_2Na]^+$, respectively. The less abundant patterns at *m*/*z* 384, 422 and 797/799 were attributed to $[\mathbf{6a}H]^+$, $[\mathbf{6a}K]^+$ and $[(\mathbf{6a})_2K]^+$, respectively. The *m*/*z* value assigned to each peak are those measured from the centroid of the ESI mass spectral envelope and are in good agreement with the calculated *m*/*z* value of the most abundant peak within each isotopic mass distribution divided by the ion charge. Both **6** and **6a** exhibit tendency to form aggregates in solution.

Regarding the process of oxidative dehydrogenation, it was observed that it occurs at room temperature and 40 °C, although with very different outcomes. In the presence of 10 mol equivalents of $H_2O_2$ in acetone at room temperature after 48 h (Fig. 11), the ESI

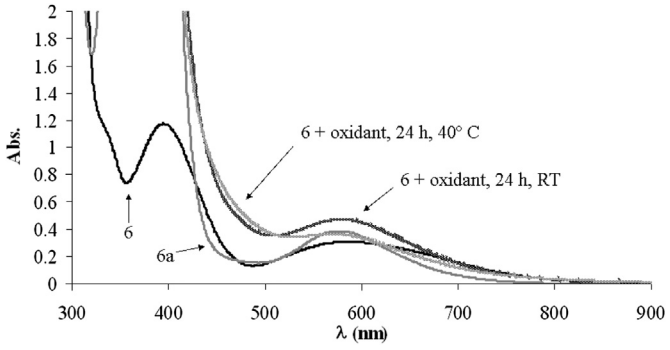


**Fig. 8.** Isotropic electronic absorption spectra of **6** (THF, 1.14 mM), **6a** (THF, 1.23 mM), **6** with 10 equiv of $H_2O_2$ after 24 h at room temperature (THF, 0.96 mM) and **6** with 10 equiv of $H_2O_2$ after 24 h at 40 °C (THF, 0.96 mM). Spectra were recorded at room temperature with 1 cm optical path quartz cells.

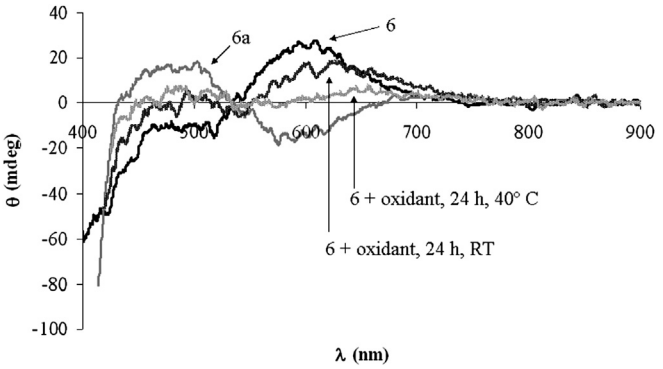


**Fig. 9.** Circular dichroism (CD) spectra of **6** (THF, 1.14 mM), **6a** (THF, 1.23 mM), **6** with 10 equiv of $H_2O_2$ after 24 h at room temperature (THF, 0.96 mM) and **6** with 10 equiv of $H_2O_2$ after 24 h at 40 °C (THF, 0.96 mM). The spectra were recorded at room temperature with 5 mm optical path quartz cells.

mass spectrum displayed signals at *m*/*z* 771/773 assigned to a protonated dimeric "half-salen" variant of **6**, referred to hereinafter as **6d**, which can also be described as $\{[Cu^{II}(H\text{-}2.1)]_2H\}^+$. Another major species with *m*/*z* 677/679 was attributed to a mono-charged dinuclear species with the formula $\{[Cu^{II}(OOH)(C_{14}H_{19}N_2O)]_2Na\}^+$. The $C_{14}H_{19}N_2O$ moiety refers to a hydrolysis product of the half-salen species which resulted in the loss of a phenolate moiety. The relative intensities of the isotopic peaks in the copper-containing species matches well the calculated isotopic distributions for a species containing two Cu atoms, as illustrated in the left inset of Fig. 11. The less abundant species with *m*/*z* 665/667 corresponds to another oxidative product matching the formula $\{[Cu^{II}(OOH)]_2[(C_{14}H_{19}N_2O)(C_{13}H_{19}N_2O)]Na\}^+$. Such tridentate species have been reported for salen-type vanadium compounds [41], hence the assumption that similar Cu-based degradation products may form under the conditions described here. More importantly, the monomeric "half-salen" variant of **6** (i.e. **6d**) was detected ($\{[Cu^{II}(H\text{-}2.1)H]\}^+$, *m*/*z* 386), clearly supporting the proposed oxidative dehydrogenation degradation pathway.

At 40 °C the degradation of **6** is faster and much more extensive (Fig. 12). Complete degradation of **6** was observed 1 h after sample preparation, leading also to the species $\{[Cu^{II}(OOH)(C_{14}H_{19}N_2O)]_2Na\}^+$ (*m*/*z* 677/679) as major oxidative product. Additional

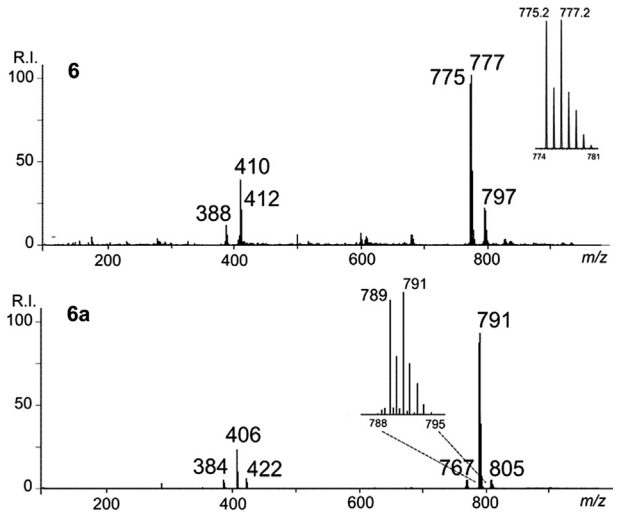


**Fig. 10.** ESI(+) mass spectra of **6** and **6a** in acetone. The inset in **6** corresponds to the calculated isotopic pattern for the dimeric species $[(\mathbf{6})_2H]^+$ whereas the inset in **6a** corresponds to the observed isotopic envelope for $[(\mathbf{6a})_2Na]^+$.

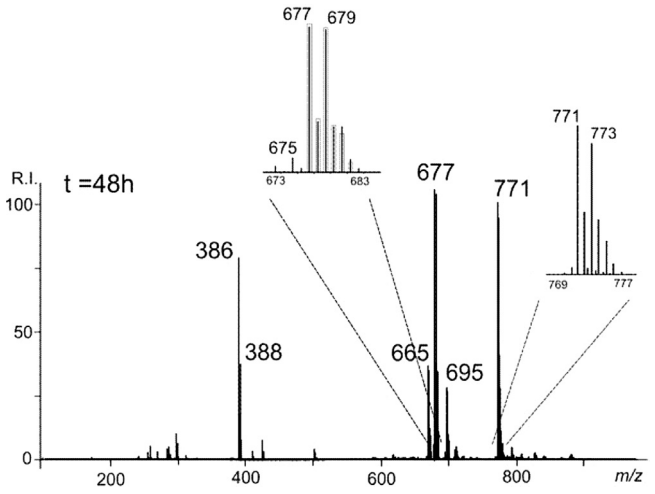


**Fig. 11.** ESI(+) mass spectrum of **6** in the presence of $H_2O_2$ in acetone, after 48 h at room temperature. Left inset: isotopic pattern match for $\{[Cu^{II}(OOH)(C_{14}H_{19}N_2O)]_2Na\}^+$. Right inset: observed peaks assigned to the "half-salen" variant of **6**, designated by **6d**.

degradation products were observed after 3 h, with the peak at *m*/*z* 114 being assigned to the protonated molecule $[(C_5H_7N)H]^+$, and the major peaks at *m*/*z* 245 and 292 being attributed to the species $[Cu^{II}(OOH)(C_5H_7N)(OH)_2H]^+$ and $[Cu^{I}(C_{14}H_{17}N_2O)]^+$, respectively. A brown precipitate formed after 5 h which prompted the addition of water to facilitate its solubilization. The spectrum obtained at 6 h show the increasing prevalence of the species at *m*/*z* 245 and *m*/*z* 292, as well as the appearance of a series of mono and double

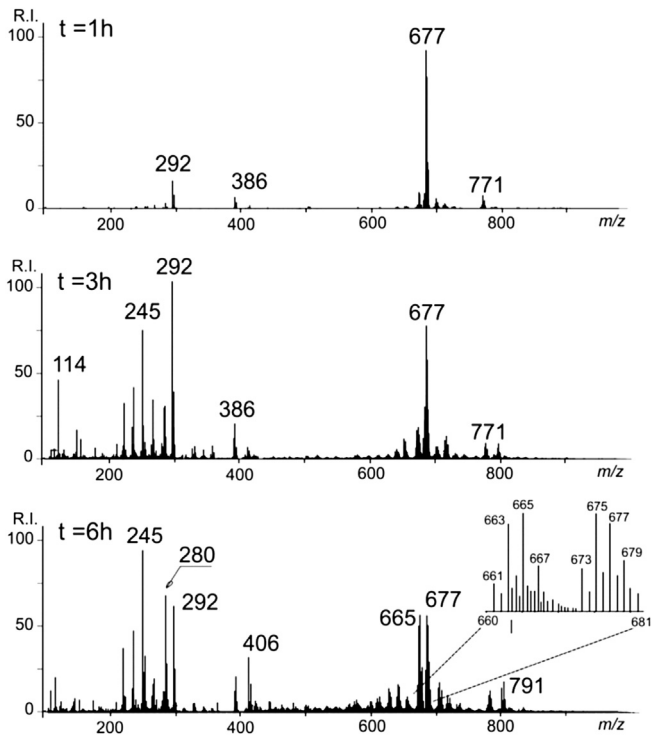


**Fig. 12.** ESI(+) mass spectra of **6** in the presence of $H_2O_2$ in acetone, at 40 °C and different times. The enlarged portion of the spectrum ($t = 6$ h) shows the overlapping of different distribution envelopes matching several species (see text). Note that the isotopic separation in the mass spectrum of 0.5 *m*/*z* units, is indicative of a doubly charged ion.

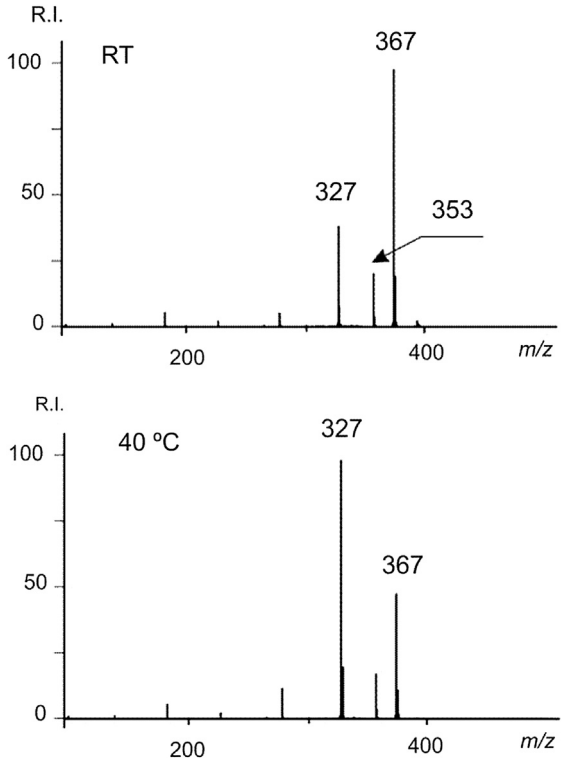


**Fig. 13.** ESI(+) mass spectra of **1** in the presence of $H_2O_2$, in acetone, after 48 h at the indicated temperatures.

charged species in the mass region 600–800 Da, in line with ongoing degradation of **6**. The enlarged portion of the spectrum shows clearly the overlapping of several species corresponding to various oxidative product matching, for example, the formulas $[Cu^{II}_4(C_{54}H_{80}N_8O_{12})(H_2O)HNa]^{2+}$ (*m*/*z* 664.1/664.5/665.1), $[Cu^{II}_2(C_{27}H_{38}N_4O_6)Na]^+$ (*m*/*z* 663/665) and $[Cu^{II}_2(C_{28}H_{38}N_4O_6)Na]^+$ with *m*/*z* 665/667.

In addition, the entire degradation process appears to be promoted by the metal center, as the free ligand precursor **1** was not oxidized and degraded in the presence of $H_2O_2$ under the same conditions (Fig. 13). Only the peaks assigned to $[\mathbf{1}H]^+$ (*m*/*z* 327), and $[\mathbf{1}Na(H_2O)]^+$ (*m*/*z* 367) were detected after 48 h at room temperature and 40 °C. Here, a less intense peak at *m*/*z* 353 was tentatively attributed to an ion with the formula $[(C_{20}H_{22}N_2O_4)H]^+$.

The interaction of **6** with an excess of hydrogen peroxide (10 equivalents in THF) was also followed by EPR. The spectrum of

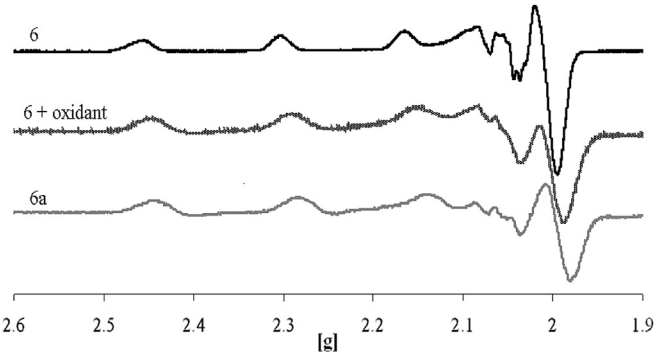


**Fig. 14.** First derivative of the X-band EPR spectra of **6**, **6a**, and **6** in the presence of 10 equiv of $H_2O_2$, measured at 77 K.

**Table 8**
Experimental spin Hamiltonian parameters for **6**, **6**/$H_2O_2$ and **6a**.

| Compound | $g_x$, $g_y$ | $A_x$, $A_y$ | $g_z$ | $A_z$ | $g_z/A_z$ |
|---|---|---|---|---|---|
| | | $\times 10^4$ cm$^{-1}$ | | $\times 10^4$ cm$^{-1}$ | cm |
| **6**[a] | 2.038, 2.057 | 36.4, 10.6 | 2.235 | 189.3 | 118 |
| **6**/$H_2O_2$[b] | 2.043 | 18.6 | 2.222 | 198.1 | 112 |
| **6a**[b] | 2.019, 2.057 | 28.1, 24.5 | 2.209 | 203.2 | 108 |

[a] EPR spectrum measured at 77 K with a 1:1 acetone:ethyleneglycol mixture as solvent.
[b] EPR spectrum measured at 77 K with THF as solvent.

**6**/$H_2O_2$ was obtained 24 h after the preparation of the sample, which was then compared with the spectra of **6** and of the $Cu^{II}$–salen compound **6a** (Fig. 14). The respective experimental spin Hamiltonian parameters are listed in Table 8.

While the three spectra are similar, the $A_z$ and $g_z/A_z$ values indicate that interaction with $H_2O_2$ did occur after a 24 h period. The result was the formation of a $Cu^{II}$ species exhibiting $A_z$ and $g_z$ values very close to **6a**. The nature of this new species can be anticipated by analyzing the Peisach–Blumberg plot [28,30]. On this basis, the following points may be emphasized: i) the replacement of the nitrogen donors by oxygen donors in a square-planar environment should cause an increase of $g_z$, which is not the case, and ii) the decrease of the $g_z/A_z$ ratio indicates that a [$N_2$,$O_2$] donor group set is maintained with an increased square-planar character. The increased planarity suggests greater structural rigidity which, under the conditions tested, can be attained by oxidative dehydrogenation of the salan ligand. This is consistent with what was observed in the ESI-MS studies.

Globally the ESI-MS, EPR, CD and UV–Vis data indicate that the $Cu^{II}$–salan compounds, in the presence of $H_2O_2$, undergo degradation by oxidative dehydrogenation of the ligand. At room temperature, the main oxidative dehydrogenation product characterized is the "half-salen" variant of **6**, designated here by **6d**.

Additionally, this degradation is promoted by the metal center, as the ligand precursors remain intact if only in the presence of $H_2O_2$ (Fig. 13). This degradation is significantly faster and more extensive at 40 °C, namely yielding tridentate ligands where one of the aromatic rings is lost. This suggests that the catalytic species involved in the sulfoxidation and alkene oxidation reactions studied here are not direct peroxido-type derivatives of the $Cu^{II}$–salan complexes, but of the $Cu^{II}$–Schiff base complexes formed in the presence of excess $H_2O_2$.

## 4. Conclusions

Five $Cu^{II}$–salan compounds were successfully prepared and characterized and their catalytic potential evaluated under mild conditions. Several of these $Cu^{II}$ compounds were characterized by single crystal X-ray diffraction studies, including a "half-salen" complex. The results obtained from the EPR studies are consistent with $Cu^{II}$ centers coordinated to mixed [N,O] donor atom sets, although individual donor atoms cannot be distinguished with certainty. Electronic absorption spectra are also consistent with phenolate-bound $Cu^{II}$ species, and circular dichroism studies showed that these compounds exhibit optical activity associated with the *d*–*d* and/or charge-transfer transitions. Remarkably, the $Cu^{II}$–salan compounds described herein undergo degradation by oxidative dehydrogenation of the ligand when in the presence of $H_2O_2$, as observed during the ESI-MS experiments and also during EPR, CD and electronic absorption studies. This degradation is significantly faster and more extensive at 40 °C. At room temperature, the main oxidative dehydrogenation product characterized is the "half-salen" variant of **6**, **6d**. Moreover, this degradation is promoted by the metal center, as the ligands precursors remain intact if only in the presence of $H_2O_2$.

This casts doubt over the true identity of the catalytic species involved in the sulfoxidation and alkene oxidation reactions. For instance, the relative inertness of the $Cu^{II}$–salan compounds in the catalytic oxidation of thioanisole and *trans*-anethole at room temperature can be explained by compounding two factors; a) the saturated coordination sphere of the $Cu^{II}$ center comprised of basic *N*- and *O*-donors; b) the lower Lewis acidity exhibited by the $Cu^{II}$ center compared to that exhibited by the $Ti^{IV}$ and $V^{V}$ analogs, which are capable of binding to $H_2O_2$ and render it electrophilic. However, knowing that extensive degradation of the $Cu^{II}$ catalyst occurs by oxidative dehydrogenation at 40 °C, the oxidations of thioanisole and *trans*-anethole, that were achieved at 40 °C, may be mediated instead by the degradation products of the initial $Cu^{II}$ complex and not involve the starting $Cu^{II}$–salan complexes. Considering that the obtained results for anethole oxidation may be the compounding of various distinct catalytic activities, it was possible to observe that the general epoxide diastereoselectivities indicate a prevalence of stepwise oxidation pathways.

The reported $Cu^{II}$–salan compounds are inactive in the oxidative coupling of 2-naphthol. This may be mostly due also to a $Cu^{II}$ center stabilized by basic *N*- and *O*-donor atoms that prevents the single-electron transfer from the naphthol to the metal center. This factor, compounded with the saturated coordination sphere of the metal center, makes the entire process of oxidative coupling difficult unless harsher conditions are used.

## Acknowledgments

This work was supported by Fundação para a Ciência e a Tecnologia (FCT), PEst-OE/QUI/UI0100/2013, the Portuguese NMR and Mass Spectrometry Networks (IST-UTL Centers, REM2013, RECI/QEQ-QIN/0189/2012 and RECI/QEQ-MED/0330/2012), grants SFRH/BD/40279/2007, SFRH/BPD/73941/2010 and SFRH/BPD/79778/2011.

## Appendix A. Supplementary material

CCDC 958111, 958112, 958067 contain the supplementary crystallographic data for this paper. These data can be obtained free of charge from The Cambridge Crystallographic Data Centre via http://www.ccdc.cam.ac.uk/products/csd/request/.

## Appendix B. Supplementary data

Supplementary data related to this article can be found at http://dx.doi.org/10.1016/j.jorganchem.2013.10.019.

## References

[1] E.I. Solomon, B.L. Hemming, D.E. Root, in: K.D. Karlin, Z. Tyeklár (Eds.), Bioinorganic Chemistry of Copper, Chapman & Hall, London, 1993.
[2] (a) I.P. Beletskaya, A.V. Cheprakov, Coord. Chem. Rev. 248 (2004) 2337–2364;
(b) H. Do, O. Daugulis, Chem. Commun. (2009) 6433–6435;
(c) C. Lin, Y. Wang, C. Fa, Eur. J. Org. Chem. (2010) 4368–4371.
[3] T. Punniyamurthy, L. Rout, Coord. Chem. Rev. 252 (2008) 134–154.
[4] G. Desimoni, G. Dusi, G. Faita, P. Quadrelli, P. Righetti, Tetrahedron 51 (1995) 4131–4144.
[5] (a) Y.N. Belokon, R.G. Davies, M. North, Tetrahedron Lett. 41 (2000) 7245–7248;
(b) Y.N. Belokon, M. North, T.D. Churkina, N.S. Ikonnikova, V.I. Maleev, Tetrahedron 57 (2001) 2491–2498;
(c) Y.N. Belokon, D. Bhave, D. D'Addario, E. Groaz, M. North, V. Tagliazucca, Tetrahedron 60 (2004) 1849–1861;
(d) T. Achard, Y.N. Belokon, J.A. Fuentes, M. North, T. Parsons, Tetrahedron 60 (2004) 5919–5930.
[6] C. Gan, G. Lai, Z. Zhang, Z. Wang, M. Zhou, Tetrahedron Asymmetry 17 (2006) 725–728.

[7] Z. Wu, L. Zhou, Z. Jiang, D. Wu, Z. Li, X. Zhou, Eur. J. Org. Chem. (2010) 4971–4975.
[8] (a) S. Bunce, R.J. Cross, L.J. Farrugia, S. Kunchandy, L.L. Meason, K.W. Muir, M. O'Donnell, R.D. Peacock, D. Stirling, S.J. Teat, Polyhedron 17 (1998) 4179–4187;
(b) H. Zhu, Z. Dai, W. Huang, K. Cui, S. Gou, C. Zhu, Polyhedron 23 (2004) 1131–1137.
[9] S. Rayati, S. Zakavi, M. Koliaei, A. Wojtczak, A. Kozakiewicz, Inorg. Chem. Commun. 13 (2010) 203–207.
[10] M.R. Maurya, B. Singh, P. Adão, F. Avecilla, J. Costa Pessoa, Eur. J. Inorg. Chem. (2007) 5720–5734.
[11] G. Rajagopal, S. Selvaraj, K. Dhahagani, Tetrahedron Asymmetry 21 (2010) 2265–2270.
[12] Y.N. Belokon, M. North, T. Parsons, Org. Lett. 2 (2000) 1617–1619.
[13] (a) P. Adão, J. Costa Pessoa, R.T. Henriques, M.L. Kuznetsov, F. Avecilla, M.R. Maurya, U. Kumar, I. Correia, Inorg. Chem. 48 (2009) 3542–3561;
(b) P. Adão, F. Avecilla, M. Bonchio, M. Carraro, J. Costa Pessoa, I. Correia, Eur. J. Inorg. Chem. (2010) 5568–5578.
[14] Y. Xiong, F. Wang, X. Huang, Y. Wen, X. Feng, Chem. Eur. J. 13 (2007) 829–833.
[15] K. Butsch, T. Günther, A. Klein, K. Stirnat, A. Berkessel, J. Neudörfl, Inorg. Chim. Acta 394 (2013) 237–246.
[16] A. Rockenbauer, L. Korecz, Appl. Magn. Reson. 10 (1996) 29–43.
[17] G.M. Sheldrick, SADABS, Program for Empirical Absorption Correction, University of Göttingen, Göttingen, Germany, 1996.
[18] M.C. Burla, R. Caliandro, M. Camalli, B. Carrozzini, G.L. Cascarano, L. De Caro, C. Giacovazzo, G. Polidori, R. Spagna, J. Appl. Cryst. 38 (2005) 381–388.
[19] G.M. Sheldrick, Acta Crystallogr. A46 (1990) 467–473.
[20] L.J. Farrugia, J. Appl. Crystallogr. 32 (1999) 837–838.
[21] (a) G.M. Sheldrick, SHELXL-97 – Programs for Crystal Structure Analysis (Release 97-2), 1998. Göttingen, Germany;
(b) G.M. Sheldrick, Acta Crystallogr. A64 (2008) 112–122.
[22] L.J. Farrugia, J. Appl. Crystallogr. 30 (1997) 565–566.
[23] C. F Macrae, P. R Edgington, P. McCabe, E. Pidcock, G.P. Shields, R. Taylor, M. Towler, J. van de Streek, J. Appl. Crystallogr. 39 (2006) 453–457.
[24] G.M. Sheldrick, SHELXS-97, Revision 5.1, University of Göttingen, Göttingen, Germany, 1997.
[25] (a) W. Sun, E. Herdtweck, F.E. Kuhn, New J. Chem. 29 (2005) 1577–1580;
(b) E.C. Constable, G. Zhang, C. E Housecroft, M. Neuburger, S. Schaffner, W.D. Woggon, New J. Chem. 33 (2009) 1064–1069.
[26] K. Bernardo, S. Leppard, A. Robert, G. Commenges, F. Dahan, B. Meunier, Inorg. Chem. 35 (1996) 387–396.
[27] M.K. Taylor, J. Reglinski, L.E.A. Berlouis, A.R. Kennedy, Inorg. Chim. Acta 359 (2006) 2455–2464.
[28] U. Sakaguchi, A.W. Addison, J. Chem. Soc. Dalton Trans. (1979) 600–608.
[29] (a) V.T. Kasumov, F. Köksal, Spectrochim. Acta A 61 (2005) 225–231;
(b) S. Deshpande, D. Srinivas, P. Ratnasamy, J. Catal. 188 (1999) 261–269;
(c) M. Valko, R. Bofa, R. Klement, J. Koziek, M. Mazfir, P. Pelikan, H. Morris, H. Elias, L. Moiler, Polyhedron 16 (1997) 903–908;
(d) R. Klement, F. Stock, H. Elias, H. Paulus, P. Pelikan, M. Valko, M. Mazur, Polyhedron 18 (1999) 3617–3628;
(e) G. Verquin, G. Fontaine, E. Abiaad, E. Zhilinskaya, A. Aboukais, J. Bernier, J. Photochem. Photobiol. B 86 (2007) 272–278;
(f) I. Sylvestre, J. Wolowska, C.A. Kilner, E.J.L. McInnes, M.A. Halcrow, Dalton Trans. (2005) 3241–3249;
(g) K.M. Ananth, M. Kanthimathi, B.U. Nair, Transition Met. Chem. 26 (2001) 333–338;
(h) I. Correia, A. Dornyei, T. Jakusch, F. Avecilla, T. Kiss, J. Costa Pessoa, Eur. J. Inorg. Chem. (2006) 2819–2830.
[30] J. Peisach, W.E. Blumberg, Arch. Biochem. Biophys. 165 (1974) 691–708.
[31] (a) R.C. Pratt, C.T. Lyons, E.C. Wasinger, T.D.P. Stack, J. Am. Chem. Soc. 134 (2012) 7367–7377;
(b) V.T. Kasumov, I. Uçar, A. Bulut, F.Z. Köksal, Naturforscher 62B (2007) 1133–1138;
(c) S. Keinan, D. Avnir, J. Chem. Soc. Dalton Trans. (2001) 941–947.
[32] (a) C.S. Schneider, J.E. Penner-Hahn, V.L. Pecoraro, J. Am. Chem. Soc. 130 (2008) 2712–2713;
(b) T.S. Smith, V.L. Pecoraro, Inorg. Chem. 41 (2002) 6754–6760;
(c) J.Y. Kravitz, V.L. Pecoraro, H.A. Carlson, J. Chem. Theory Comput. 1 (2005) 1265–1274;
(d) D. Balcells, F. Maseras, G. Ujaque, J. Am. Chem. Soc. 127 (2005) 3624–3634;
(e) D. Balcells, F. Maseras, A. Lledós, J. Org. Chem. 68 (2003) 4265–4274;
(f) M.L. Kuznetsov, J. Costa Pessoa, Dalton Trans. (2009) 5460–5468;
(g) M.R. Maurya, A. Arya, A. Kumar, M.L. Kuznetsov, F. Avecilla, J. Costa Pessoa, Inorg. Chem. 49 (2010) 6586–6600;
(h) S. Barroso, P. Adão, F. Madeira, M.T. Duarte, J. Costa Pessoa, A.M. Martins, Inorg. Chem. 49 (2010) 7452–7463;
(i) M.R. Maurya, M. Bisht, A. Kumar, M.L. Kuznetsov, F. Avecilla, J. Costa Pessoa, Dalton Trans. 40 (2011) 6968–6983;
(j) M.R. Maurya, P. Saini, A. Kumar, J. Costa Pessoa, Eur. J. Inorg. Chem. (2011) 4846–4861;
(k) M.R. Maurya, C. Haldar, A.A. Khan, A. Azam, A. Salahuddin, A. Kumar, J. Costa Pessoa, Eur. J. Inorg. Chem. (2012) 2560–2577.
[33] (a) I. Ryu, J. Seo, Y. Lee, Y. Lim, J. Ahn, H. Hur, J. Agric. Food Chem. 53 (2005) 5954–5958;
(b) D. Carteau, P. Brunerie, B. Guillemat, D.M. Bassani, Photochem. Photobiol. Sci. 6 (2007) 423–430.
[34] (a) A.S. Capes, A.T. Crossman, L.A. Webster, M.A.J. Ferguson, I.H. Gilbert, Tetrahedron Lett. 52 (2011) 7091–7094;
(b) J. Barluenga, H. Vázquez-Villa, A. Ballesteros, J.M. González, Org. Lett. 4 (2002) 2817–2819;
(c) M.L. Kantam, B. Neelima, C.V. Reddy, R. Chakravarti, Ind. Eng. Chem. Res. 46 (2007) 8614–8619;
(d) D. Jiang, T. Mallat, F. Krumeich, A. Baiker, J. Catal. 257 (2008) 390–395;
(e) M. Kokubo, T. Naito, S. Kobayashi, Tetrahedron (2010) 1111–1118;
(f) A. Kamal, R. Ramu, M.A. Azhar, G.B.R. Khanna, Tetrahedron Lett. 46 (2005) 2675–2677.
[35] L.C. Carvalho do Lago, A.C. Matias, C.S. Nomura, G. Cerchiaro, J. Inorg. Biochem. 105 (2011) 189–194.
[36] J. Labuda, P. Tarapcik, A. Kotocová, J. Sima, Monatsh. Chem. 123 (1992) 693–699.
[37] T. Hamada, H. Ishida, S. Usui, Y. Watanabe, K. Tsumura, K. Ohkubo, J. Chem. Soc. Chem. Commun. (1993) 909–911.
[38] (a) X. Li, J. Yang, M. Kozlowski, Org. Lett. 3 (2001) 1137–1140;
(b) V.B. Sharma, S.L. Jain, B. Sain, J. Mol. Catal. A-Chem. 219 (2004) 61–64;
(c) T. Temma, S. Habaue, Tetrahedron Lett. 46 (2004) 5655–5657;
(d) T. Temma, B. Hatano, S. Habaue, Tetrahedron 62 (2006) 8559–8563;
(e) T. Temma, Y. Takahashi, S. Habaue, Tetrahedron 48 (2007) 7301–7304;
(f) S. Sabarinathan, G. Vasuki, P.S. Rao, Eur. J. Chem. 4 (2010) 360–367.
[39] J.M. Brunel, Chem. Rev. 105 (2005) 857–897.
[40] (a) M. Arca, G. Azimi, F. Demartin, F.A. Devillanova, L. Escriche, A. Garau, F. Isaia, R. Kivekas, V. Lippolis, V. Muns, A. Perra, M. Shamsipur, L. Sportelli, A. Yari, Inorg. Chim. Acta 358 (2005) 2403–2412;
(b) G. Saha, K.K. Sarkar, T.K. Mondal, C. Sinha, Inorg. Chim. Acta 387 (2012) 240–247.
[41] P. Adão, M.R. Maurya, U. Kumar, F. Avecilla, R.T. Henriques, M.L. Kuznetsov, J. Costa Pessoa, I. Correia, Pure Appl. Chem. 81 (2009) 1279–1296.